Cerebral Cortex Advance Access published October 14, 2014

OXFORD

Cerebral Cortex, 2014, 1–11

doi: 10.1093/cercor/bhu243
ORIGINAL ARTICLE

ORIGINAL ARTICLE

Developmental Sculpting of Intracortical Circuits by MHC Class I H2-Db and H2-Kb

Jaimie D. Adelson[1], Richard W. Sapp[1], Barbara K. Brott[1], Hanmi Lee[1], Kazunari Miyamichi[2], Liqun Luo[2], Sarah Cheng[1], Maja Djurisic[1] and Carla J. Shatz[1]

[1]Departments of Biology and Neurobiology and Bio-X and [2]Department of Biology, Stanford University, Stanford, CA 94305, USA

Address correspondence to Jaimie D. Adelson, 318 Campus Drive W1.1, Stanford, CA 94305, USA. Email: jaimie.adelson@gmail.com; Carla J. Shatz. 318 Campus Drive W1.1, Stanford, CA 94305, USA. Email: cshatz@stanford.edu

Abstract

Synapse pruning is an activity-regulated process needed for proper circuit sculpting in the developing brain. Major histocompatibility class I (MHCI) molecules are regulated by activity, but little is known about their role in the development of connectivity in cortex. Here we show that protein for 2 MHCI molecules H2-Kb and H2-Db is associated with synapses in the visual cortex. Pyramidal neurons in mice lacking H2-Kb and H2-Db (KbDb KO) have more extensive cortical connectivity than normal. Modified rabies virus tracing was used to monitor the extent of pyramidal cell connectivity: Horizontal connectivity is greater in the visual cortex of KbDb KO mice. Basal dendrites of L2/3 pyramids, where many horizontal connections terminate, are more highly branched and have elevated spine density in the KO. Furthermore, the density of axonal boutons is elevated within L2/3 of mutant mice. These increases are accompanied by elevated miniature excitatory postsynaptic current frequency, consistent with an increase in functional synapses. This functional and anatomical increase in intracortical connectivity is also associated with enhanced ocular dominance plasticity that persists into adulthood. Thus, these MHCI proteins regulate sculpting of local cortical circuits and in their absence, the excess connectivity can function as a substrate for cortical plasticity throughout life.

Key words: activity-dependent development, horizontal connections, major histocompatibility complex class I, modified rabies circuit tracing, visual cortex

Introduction

Intracortical circuits are sculpted by neural activity and experience during developmental critical periods (Katz and Shatz 1996), and retain a more limited ability to remodel during maturity (Knudsen 2004). In many binocular animals, L2/3 and L5 pyramidal neurons in visual cortex extend long horizontal axons laterally up to a few millimeters away as well as across the corpus callosum, connecting functionally relevant subsets of neurons to each other (Livingstone and Hubel 1984; Gilbert and Wiesel 1989; Gilbert 1992; Kenan-Vaknin et al. 1992; Salin and Bullier 1995; Trachtenberg and Stryker 2001; Tanigawa et al. 2005; Van Hooser et al. 2006). Initially, in the visual cortex, these axons are exuberant (Callaway and Katz 1990). During the critical period, these horizontal connections are pruned in a process requiring visual experience (Callaway and Katz 1991) and neural activity (Gilbert and Wiesel 1989; Callaway and Katz 1990; Lund et al. 1993; Malach et al. 1993; Durack and Katz 1996; Ruthazer and Stryker 1996). Dendrites and spines in many regions of the brain also undergo an activity-regulated period of growth, followed by retraction (Cline 2001; Sin et al. 2002; Vaillant et al. 2002; Hofer et al. 2006a, 2006b; De Marco García et al. 2011; Chen et al. 2012). In the adult, anatomical changes in horizontal connections in

response to alterations in visual input, though more restricted, can still occur following manipulations such as retinal lesions (Keck et al. 2008; Palagina et al. 2009; Yamahachi et al. 2009), consistent with the idea that anatomical changes in connectivity underlie experience-dependent functional plasticity.

Ocular dominance (OD) plasticity is one form of experience-dependent synaptic plasticity. When one eye is closed or removed, the deprived eye loses the ability to activate cortical neurons, which become more responsive to the open eye (Wiesel and Hubel 1963; Hubel et al. 1977). During the critical period, visual deprivation causes a strong shift in the OD of cortical neurons toward the open eye (Hubel et al. 1977; Shatz 1990; Gordon and Stryker 1996; Frenkel and Bear 2004). In adult visual cortex, OD plasticity can be elicited but requires significantly longer periods of monocular deprivation (MD; Tagawa et al. 2005; Sato and Stryker 2008). Many studies have identified molecular mechanisms that contribute to activity-dependent synaptic plasticity in the visual cortex (Hensch 2005; Flavell and Greenberg 2008; Tropea et al. 2009; Levelt and Hübener 2012), but the link from candidate molecules to experience-dependent structural change has not been explored as extensively.

One set of candidate molecules that could link activity-dependent structural changes to alterations in synaptic and circuit-level plasticity are the major histocompatibility class I (MCHI) genes, which were discovered in a screen for activity-regulated genes in the developing visual system (Corriveau et al. 1998; Shatz 2009; Elmer and McAllister 2012). In the developing lateral geniculate nucleus (LGN) of the thalamus, neural activity is known to be required for synapse pruning and eye-specific layer formation (Huberman et al. 2008). Just 2 of the over 50 MHCI genes, H2-Kb and H2-Db, are known to regulate synapse pruning via alterations in synaptic learning rules and glutamate receptor subunit composition at retinogeniculate synapses (Lee et al. 2014). Mice lacking both H2-Kb and H2-Db (KbDb KO) have less synapse elimination compared with wild type (WT), and elimination can be restored to WT levels by selectively expressing H2-Db in LGN neurons (Lee et al. 2014). H2-Kb and H2-Db are both also expressed in cortical neurons including pyramidal cells (Huh et al. 2000; Datwani et al. 2009). During the critical period in the visual cortex, KbDb KO mice have enhanced OD plasticity, as assessed by measuring open eye strengthening following MD (Datwani et al. 2009; Shatz 2009). In vitro studies on β2m/Tap1 KO mice, which lack surface expression of the vast majority of MHCI proteins, reveal an increase in synapse density, while over expression of H2-Kb in vitro resulted in a decrease in synapse density (Goddard et al. 2007; Glynn et al. 2011); both observations are consistent with the idea that these MHCI proteins contribute to synapse pruning. Here, we examined whether the specific MHCI molecules H2-Kb and H2-Db also regulate developmental sculpting of intracortical connectivity in vivo in the visual cortex.

Materials and Methods

Animals

KbDb KO mice, offspring of breeding pairs on a C57BL/6 background, were originally generously provided by H. Ploegh and are now maintained in our colony (Cambridge, MA, USA; Vugmeyster et al. 1998). C57BL/6 (i.e., KbDb WT) controls were purchased (Charles River) or bred in Stanford facilities. For modified rabies virus circuit tracing experiments, CaMK2α-CreER; CAG-stop-tTA2 double transgenic mice were provided by L. Luo (Miyamichi et al. 2011; Stanford, CA, USA) and bred to KbDb KO mice. F1 generation CaMK2α-CreER; CAG-stop-tTA2; $KbDb^{+/-}$ mice were bred to $KbDb^{+/-}$ mice to produce F2 experimental animals (CaMK2α-CreER; CAG-stop-tTA2; $KbDb^{+/+}$ or $KbDb^{-/-}$), control animals (CAG-stop-tTA2; $KbDb^{+/+}$ or $KbDb^{-/-}$), and breeders (CaMK2α-CreER; CAG-stop-tTA2; $KbDb^{+/-}$). All mice were maintained in a pathogen-free environment. All experiments using animals were performed blind to the genotype and in accordance with a protocol approved by the Stanford University animal care and use committee and in keeping with the National Institutes of Health *Guide for the Care and Use of Laboratory Animals*.

Retrograde Circuit Tracing with Modified Rabies Virus

See Figure 1A and Supplementary Figure 1 for diagrams and complete description of methods, respectively. All handling of rabies virus followed procedures approved by Stanford University's Administrative Panel on Biosafety (APB) for Biosafety Level 2. pAAV2 TRE-histone-mCherry-2a-TVA-2a-RG (TRE-mCTG) was constructed by replacing GFP-coding sequence of TRE-HTG (Miyamichi et al. 2011) with that of mCherry by using PCR-based cloning. Recombinant adeno-associated virus (AAV; serotype 2) was produced in the University of North Carolina viral core. Mice were injected IP with 0.1 mg Tamoxifen Free Base (Sigma, T5648) suspended in 2% ethanol and 98% corn oil (Sigma, 63156) at P10–P14. At P21–P23, mice were injected with 150 nL of AAV2 TRE-mCTG. Mice were placed in a Kopf stereotaxic set-up under approximately 1–2% isoflurane inhalable anesthesia. AAV was injected using a NanoFil 34–36 gauge beveled syringe (Nanofil-100, World Precision Instruments) at 50 nL/min into visual cortex through a small drill hole (coordinates: +2.25 mm lateral, 3.4 mm posterior to Bregma, −0.5 mm depth from brain surface). Fourteen days after AAV injection (P35–P37), mice were injected at 50 nL/min with 150 nL rabies-dG-GFP + EnvA [prepared according to the protocol (Osakada and Callaway 2013) or purchased from Salk Institute Viral Core], through the same drill hole as for AAV injection. Note that the volumes of injected virus were small (150 nL) to restrict the number of starter cells and the location of starter cells to a local region of visual cortex, permitting connections within visual cortex to be analyzed. In addition, to validate this retrograde tracing method, which previously had only been used for long distance connectivity (Miyamichi et al. 2011), in one additional experiment, much larger injections were made (1000 nL of each virus) and retrograde labeling in LGN and contralateral visual cortex was assessed. Five days after the modified rabies injection (P40–P42), animals were deeply anesthetized and perfused with ice-cold PBS and 4% paraformaldehyde. Coronal sections of visual cortex were cut at 50 μm thickness using a Leica VT1200S vibratome (Leica Microsystems, Inc., IL, USA) and mounted on slides with ProLong Gold Anti-Fade Reagent (Life Technologies, CA, USA).

Horizontal Connectivity Analysis

The number of "starter cells" was counted for each analyzed animal, where a starter cell is defined as a neuron infected by both AAV and modified rabies virus, determined by co-localization of mCherry and GFP (Fig. 1A and Supplementary Fig. 1). The number of GFP-labeled long-range presynaptic partners was counted, defined as cells falling outside of 250 μm laterally from the injection site. Total connectivity was determined by counting all GFP-labeled cells, dividing by the number of starter cells, and subtracting the average background number of GFP-labeled cells observed in control Cre^{-} mice. Counting of GFP-labeled cells was initiated in the furthest posterior coronal section of visual cortex containing a starter cell and all subsequent anterior sections of cortex

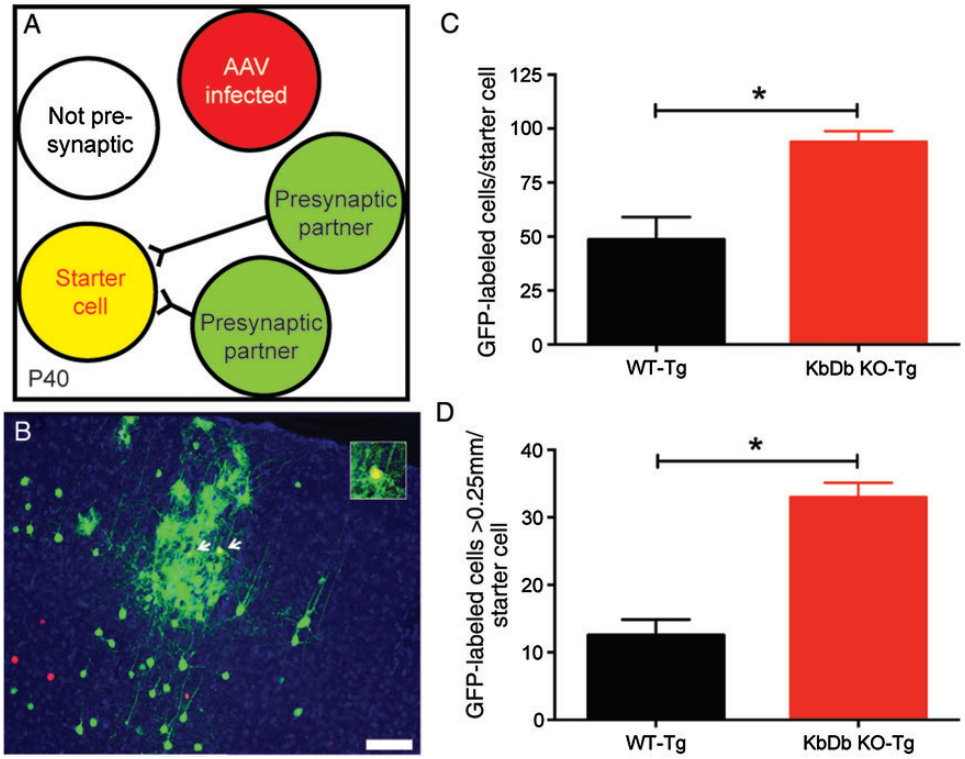

Figure 1. Modified rabies tracing reveals a higher number of connected neurons in KbDb KO-Tg visual cortex. (*A*) Diagram of modified rabies viral tracing method and (*B*) example of resulting cellular labeling. Yellow: starter cells, double-labeled with GFP and mCherry; white arrows point to 2 starter cells. Inset in *B*: higher magnification view of a starter cell. Green: rabies-infected presynaptic partners of starter cells labeled with GFP only. Red: AAV-infected histone-mCherry-labeled cells, with fluorophore labeling only in nucleus (Supplementary Fig. 1). (*C*) Histograms showing total number of GFP-labeled presynaptic cells in WT-Tg versus KbDb KO-Tg, normalized to the number of starter cells. WT-Tg: 48.4 ± 10.7 cells, KO-Tg: 93.7 ± 5.2 cells; $P = 0.04$. (*D*) The number of GFP-labeled cells >250 μm from the injection site was counted and normalized to the number of starter cells. WT-Tg: 12.5 ± 2.4 GFP-labeled cells/starter cell; KO-Tg: 32.9 ± 2.2 GFP-labeled cells/starter cell; $P = 0.03$. $N = 5$ WT-Tg and 3 KO-Tg animals. Mann–Whitney *U*-test used for *C* and *D*. Error bars = SEM. Scale bar = 100 μm. Analysis carried out at P40.

(both hemispheres; including the sparse long-range labeling observed in contralateral visual cortex, and somatosensory and auditory cortex).

Dendritic Complexity and Spine Density Analyses

Dendritic complexity was assessed using Sholl analysis (Sholl 1953). Isolated GFP-labeled excitatory pyramids in L2/3 were imaged using a Prairie 2-photon microscope for dendritic morphology analysis. Cells were identified as excitatory based on morphology, and imaged if at least 75 μm continuous basal and/or apical dendrites proximal to the cell body were in the plane of sectioning. We focused specifically on an analysis of proximal dendrites because these receive the bulk of intracortical horizontal connections from other pyramidal cells (Gilbert and Wiesel 1989; Thomson and Bannister 2003; Feldmeyer et al. 2006). Imaging was carried out with a ×63 water immersion objective corrected for slide thickness, and a ×1 zoom for full cell imaging, and a ×4 zoom for dendrite imaging (51μm × 51 μm field of view). Dendritic morphology was analyzed by reconstructing cells with Fiji's "Simple Neurite Tracer" followed by Fiji's Sholl analysis of dendrites belonging to identified pyramidal neurons in 50-μm thick visual cortex slices.

Axon Bouton Analysis

Biotinylated dextran amine (BDA) was used for anterograde labeling of horizontal axonal projections in L2/3 of visual cortex (as described by Veenman et al. 1992). Stereotaxic surgeries were performed on a Kopf stereotaxic set-up. At P26 or P27, mice were anesthetized with approximately 2.5% isoflurane and a small hole was drilled into the skull in visual cortex (relative to Bregma. X: −3.4 mm, Y: −2.25 mm, Z: −0.5 mm). A small needle was used to pierce the dura, and 200 nL of BDA (10 000 MW, NeuroTrace BDA-10 000 Neuronal Tracer Kit, Molecular Probes, Eugene, OR, USA) was injected into each site using a NanoFil syringe (World Precision Instruments, Inc., Sarasota, CA, USA). After 14 days (P40–P41), mice were deeply anesthetized and perfused, brains were removed and 50 μm coronal sections were cut using a vibratome (VT 1000 S; Leica Microsystems, Wetzlar, Germany). Sections were incubated with 0.6 μg/mL of avidin–horseradish peroxidase (NeuroTrace BDA-10 000 Neuronal Tracer Kit) for 2.5 h, reacted with 1% diaminobenzidine to visualize tracer, and mounted on slides. Sections were imaged at ×10 using bright-field microscopy (Nikon Eclipse E800, Melville, NJ, USA). The density of en passant boutons in visual cortex ipsilateral to the injection site was assessed using ImageJ.

Visual Cortex Slice Physiology

Cortical slices and physiology were carried out as in Goddard et al. (2007) and Lee et al. (2014). After brief intracardinal perfusion of ice-cold ACSF (in mM; 125 NaCl, 26 $NaHCO_3$, 2.3 KCl, 1.26 KH_2PO_4, 1.3 $MgCl_2$, 2.5 $CaCl_2$, and 10 glucose, aerated with 95% O_2/5% CO_2), brains from P26 to P31 male mice were removed and coronal sections (400 μm) including visual cortex were made using a vibratome (Leica VT1000S, Leica Microsystems, Inc., IL, USA) in ice-cold NMDG solution (in mM: 135 NMDG, 1 KCl, 1.2 KH_2PO_4, 1.5 $MgCl_2$, 0.5 $CaCl_2$, 20 choline bicarbonate,

and 10 glucose). Sections were transferred to a recovery chamber containing ACSF at 37 °C for 30 min and at room temperature for an additional 30 min before recordings. Whole-cell patch-clamp recordings were performed from pyramidal neurons in layer 2/3 of visual cortex. Recording pipette (2–4 MΩ) contained Cs^+-based internal solution (in mM: 105 CsCl, 20 TEA-Cl, 2 $MgCl_2$, 1 EGTA, 10 HEPES, 3 Mg-ATP, 15 phosphocreatine, 1 Na-GTP, 5 QX-314, pH 7.4, and 280 mOsm). Miniature excitatory postsynaptic currents (mEPSCs) were isolated by applying TTX (1 µM, Sigma), SR95531 (20 µM; Tocris) to block $GABA_A$ receptors, and APV (100 µM; Tocris) to block NMDA receptors. All recordings were done at 30–32 °C in a chamber with constant ACSF flow. Synaptic responses were recorded using an Axopatch 200B amplifier (Molecular Devices, CA, USA), digitized using Digidata 1322A (Axon Instruments, CA, USA), and data acquisition was performed by Clampex 9.2 (Axon Instrument, CA, USA). Data analysis was conducted using the MiniAnalysis software (ver. 6.0.7, Synaptosoft).

Synaptosome Preparation and Western Blots

Synaptosome preparations and western blots for H2-Kb and pan-Kb/Db were carried out as detailed in Adelson et al. (2012). Synaptosome-enriched fractions were prepared as described (Johnson et al. 1997; Yin et al. 2002). Briefly, freshly isolated brain hemispheres were homogenized by 12 strokes of a Dounce homogenizer in homogenization buffer (10 mM HEPES pH 7.3, 0.5 mM EGTA, 33% sucrose, 4 mM Pefabloc SC PLUS (Roche), and 0.2 mM phenylmethanesulfonyl fluoride), and centrifuged for 10 min at $2000 \times g$. Supernatants were passed through three-layered 100 µm pore nylon membranes, and then passed through 5 µm nitrocellulose filters. For further purification to synaptosomes, filtrates were centrifuged at $10\,000 \times g$ for 10 min, and pellets were resuspended in homogenization buffer and SDS–PAGE sample buffer. Antibodies against H2-Kb and H2-Kb/Db were used at 1 : 500 dilution (Adelson et al. 2012; Lee et al. 2014). Samples were then electrophoresed on an SDS–PAGE gel, transferred to the Immobilon-P PVDF transfer membrane (Millipore), and western blotted with rabbit monoclonal antibodies to H2-Kb or H2-Db/Kb, at a dilution of 1 : 500.

Enucleations and Arc mRNA Induction

Enucleations and Arc mRNA induction were performed as detailed in Tagawa et al. (2005). Briefly, KbDb KO and WT controls were monocularly enucleated at P100 (monocular enucleation treatment group) or P109 (normally reared treatment group) using 2–3% isoflurane anesthesia. Eyelids were sealed with Vetbond tissue adhesive glue (3M, St Paul, MN, USA). All mice were placed in total darkness for 16 h overnight at P109. At P110, mice were exposed to bright light for 30 min, followed by anesthesia with 3% isoflurane and immediate brain removal. Brains were embedded in Thermo Scientific's M-1 Embedding Matrix for frozen sectioning and frozen using 100% ethanol and dry ice, stored at 80 °C, and sectioned at 16 µm on a Thermo Scientific Shandon cryostat.

Isotopic In Situ, Autoradiography, and Analysis

Isotopic in situ hybridization for Arc mRNA was performed as previously described (Lein and Shatz 2000; Tagawa et al. 2005) using an isotopic (S^{35}) probe that hybridized to Arc mRNA (generated from full-length mouse Arc cDNA, gift of P. Worley, Johns Hopkins University, Lyford et al. 1995). Autoradiography in photographic emulsion was allowed to develop for 2–3 days before development. Analysis of signal was accomplished using the Neurolens software (version 1.7.3, Massachusetts General Hospital, Université de Montréal et CRIUGM; neurolens.org).

Results

Modified Rabies Virus Circuit Tracing Reveals Greater Density of Intracortical Pyramidal Neuron Connectivity in KbDb KO Visual Cortex

To address whether H2-Kb and H2-Db regulate patterns of horizontal connectivity in cortex, we employed a modified rabies virus tracing method. By using a combined transgenic and viral vector approach, modified rabies virus circuit tracing can identify a small subset of starter cells, as well as their presynaptic partners that get labeled transynaptically via rabies virus infection, which crosses the synapse retrogradely from the starter cells (Fig. 1A; Supplementary Fig. 1; Wickersham et al. 2007; Wall et al. 2010; Miyamichi et al. 2011). This method was initially developed to examine long-range patterns of connectivity in the olfactory system (Miyamichi et al. 2011). Here, we employ it in a new application to examine intracortical patterns of connectivity in WT and KbDb KO mice within a single cerebral cortical area.

To study connectivity of the CaMK2α$^+$ pyramidal neurons primarily responsible for the horizontal connections in visual cortex (Gilbert and Wiesel 1989; Thomson and Bannister 2003; Feldmeyer et al. 2006), WT or KbDb KO mice were generated on a transgenic background needed for rabies tracing. A transgenic line (Tg) carrying ubiquitous expression of a tetracycline transactivator element (tTA2) under transcriptional control of a floxed stop cassette (CAG-stop-tTA2), as well as Cre fused to an estrogen receptor with a CaMK2α promoter (CaMK2α-CreER; Miyamichi et al. 2011), was used (see Materials and Methods); this line, henceforward called the transgenic line (Tg), was crossed to WT and KbDb KO mice, generating WT-Tg and KbDb KO-Tg mice used here. In these mice, tamoxifen administration (P10–P14) activates Cre, inducing the expression of tTA2 only in CaMK2α$^+$ pyramidal neurons. One week later, when tTA2 is well expressed (Miyamichi et al. 2011), an AAV was stereotaxically injected into visual cortex under the control of a tetracycline-response element (TRE), causing the production of histone-mCherry as well as the avian receptor TVA (Barnard et al. 2006), and rabies glycoprotein (RG) in infected CaMK2α$^+$ cells. Two weeks later at P35, a modified rabies virus expressing GFP and the avian envelope protein EnvA (which recognizes and selectively infects TVA$^+$ cells) was stereotaxically injected into the same region of visual cortex. Cells infected with both AAV and modified rabies virus are termed "starter cells," identified by co-labeling of histone-mCherry and GFP. The AAV-provided RG protein (needed for synapse jumping) allowed the rabies virus to travel retrogradely to presynaptic partner cells (GFP-labeled only). Cortical connectivity in WT-Tg and KbDb KO-Tg was assessed 5 days after rabies infection, at P40.

To validate methodology in WT-Tg mice, we first demonstrated the presence of AAV-infected histone-mCherry-labeled cells, modified rabies-infected GFP-labeled cells, and the "starter cells" in which both fluorophores are colocalized, rendering them yellow (Fig. 1B). A low dose of tamoxifen that did not cause significant body weight change (Materials and Methods; Supplementary Fig. 2A) was used to activate Cre. At the site of the injection, control mice lacking Cre never had AAV-infected mCherry-labeled cells, and only a low level of rabies-infected GFP-labeled cells, likely due to slight leakiness of the TRE promoter (Miyamichi et al. 2011). The number of GFP-labeled cells

was very low compared with that seen in experimental animals receiving modified rabies infection (Supplementary Fig. 2B). To assess background labeling, the total number of GFP-labeled cells in control mice lacking Cre (Cre^-) was counted and the average background number of GFP-labeled cells was determined to be 95 ± 38 GFP-labeled cells (mean + SEM), very low as compared with the average of 1046 ± 201 GFP-labeled cells in Cre^+ experimental animals (Supplementary Fig. 2B). Because the number of labeled cells in Cre^+ experimental animals was over 10 times greater than Cre^- controls ($P = 0.002$), the density of local connectivity can be reliably assessed—possibly even underestimated. We further verified that the presence of $CaMK2\alpha^+$ starter cells in visual cortex results in long distance retrograde labeling of neurons in brain regions known to send projections to visual cortex, including contralateral visual cortex and LGN. Callosally projecting neurons and their terminations are primarily located in a zone at the V1/V2 border (Olavarria and Van Sluyters 1985), and because we purposefully labeled a very small number of starter cells, many are not in locations where they would receive callosal connections. Similarly, the majority of LGN neurons project to the stellate neurons of Layer 4, and starter cells were primarily located in L2/3 and L5 using this transgenic mouse line with a CaMK2α promoter. Therefore, in a separate experiment, large volumes of the viruses were injected to label hundreds of starter cells for this proof-of-principle experiment (see Materials and Methods). As expected (Miyamichi et al. 2011), rabies-infected GFP-labeled presynaptic neurons were then detected in LGN as well as in the contralateral hemisphere (Supplementary Fig. 2C). GFP-labeled cells were also observed in ipsilateral visual cortex millimeters away from starter cells, consistent with known long-range horizontal connections in L2/3 and L5. Control mice lacking Cre did not have labeling in any of these regions.

After validating the reliability of the modified rabies virus method, connectivity in KbDb KO visual cortex was assessed. $CaMK2\alpha^+$ starter cells in L2/3 and L5 of visual cortex were visualized (range of 8–56 starter cells per animal; no significant difference in the number of starter cells in WT-Tg vs. KbDb KO-Tg; WT-Tg: 24 ± 19, KO-Tg: 12 ± 10 cells, mean ± SD, $P = 0.2$). To determine whether connectivity is greater in KbDb KO mice, the total number of GFP-labeled cells normalized to the number of starter cells was determined for each animal. The number of all presynaptic cortical neurons per starter cell was almost twice as great in KbDb KO-Tg mice compared with WT-Tg (Fig. 1C; WT-Tg: 48.4 ± 10.7 cells, KO-Tg: 93.7 ± 5.2 cells; $P < 0.05$). To determine whether longer range horizontal connectivity contributes to this increase, just presynaptic GFP-labeled cells >250 μm from the injection site were analyzed (Fig. 1D). KbDb KO-Tg mice had a 2.6-fold increase in the number of long-range cortical L2/3 and L5 presynaptic partners per starter cell compared with WT-Tg (Fig. 1D; WT-Tg: 12.5 ± 2.4 presynaptic GFP-labeled cells, KO-Tg: 32.9 ± 2.2 presynaptic GFP-labeled cells; $P < 0.05$). These observations suggest that developmental pruning of intralaminar axonal projections and/or synapses of L2/3 and L5 cortical neurons is disrupted in KbDb KOs.

KbDb KO L2/3 Pyramidal Cells Have More Complex Basal Dendrites and Elevated Spine Density

Pyramidal neurons in L2/3 and L5 of visual cortex are more extensively interconnected in KbDb KO mice. It is possible that not only the degree of connectivity differs, but also dendritic branching patterns and spine density, both of which are known to be regulated by neural activity and visual experience (Sin et al. 2002; Hofer et al. 2009). Modified rabies infection extensively and brightly labels neuronal processes, making it a useful method for analysis of morphology. Dendritic branching and spine density were therefore analyzed on apical and basal dendrites proximal to the soma of isolated GFP-labeled L2/3 pyramids (Fig. 2A, B). Dendrites were analyzed if a continuous length originating from the soma of ≥75 μm could be traced (average segment length: basal = 206 ± 13 μm; apical including side branches = 238 ± 22 μm). Dendritic branching complexity was assessed by reconstructing individual L2/3 pyramidal cells for Sholl analysis (Fig. 2A). The basal dendrites of KbDb KO-Tg cells had more complex branching (Fig. 2C; $P < 0.0001$; $N = 9$ WT-Tg and 11 KO-Tg cells), but the apical dendrites were indistinguishable from WT-Tg (Fig. 2D; $P = 0.21$; $N = 9$ WT-Tg and 10 KO-Tg cells).

Next, the postsynaptic components of excitatory synapses—the dendritic spines (Yuste and Bonhoeffer 2001; Nimchinsky et al. 2002)—were also analyzed along apical and basal dendrites of GFP-labeled L2/3 pyramids (Fig. 2B). Spine density along basal dendrites was increased in KbDb KO-Tg mice by about 10% over WT-Tg (Fig. 2E; WT-Tg: 6.8 ± 0.5 spines/10 μm, $N = 11$ cells, 1990 total spines; KO-Tg: density = 7.4 ± 0.3 spines/10 μm, $N = 18$ cells, 3784 total spines; $P = 0.03$). No difference in spine density was observed on apical dendrites (Fig. 2F; WT-Tg: 7.2 ± 0.8 spines/10 μm, $N = 9$ cells, 1365 total spines; KO-Tg: density = 7.7 ± 0.4 spines/10 μm; $N = 12$ cells, 2399 total spines; $P = 0.84$). There was no observed difference in spine type distribution along either basal or apical dendrites (Supplementary Fig. 3).

Bouton Density Is Elevated Along Axons Projecting to L2/3, and the Frequency of mEPSCs Recorded From L2/3 Pyramidal Cells Is Elevated, in KbDb KO Cortex

The increases observed in basal dendritic complexity and spine density in KbDb KO L2/3 pyramids imply that there might also be changes in presynaptic axons, such as an increase in the density of presynaptic axonal boutons. Small quantities of the anterograde tracer BDA were injected in the visual cortex to visualize axons of labeled cells (Fig. 3A). Bouton density along labeled axons running in L2/3 was significantly elevated in KbDb KO visual cortex compared with WT (WT: 6.7 ± 0.7 boutons/10 μm; KO: 11.0 ± 1.5 boutons/10 μm, $P = 0.01$; Fig. 3B,C). These experiments were performed in WT and KbDb KO mice. This approach not only provides information about axon bouton density, but also provides a measure of changes in connectivity independent of the transgenic line used above for the rabies tracing method.

To determine whether the increased density of both boutons and spines present in KbDb KOs reflects a greater number of functional inputs, whole-cell recordings from L2/3 pyramids in WT and KbDb KO visual cortex were used to measure mEPSCs (Fig. 3D). KO mEPSC frequency was elevated relative to WT (WT: 1.4 ± 0.2 Hz; KO: 2.9 ± 0.6 Hz, $P = 0.02$; Fig. 3E), whereas mEPSC amplitude was similar between genotypes (WT: 19.7 ± 0.7 pA; KO: 18.9 ± 0.7 pA, $P = 0.19$; Fig. 3F). The presence of elevated mEPSC frequency is consistent with the idea that KO L2/3 pyramids receive more functional excitatory synaptic inputs than WT, whereas the similar mEPSC amplitudes suggests that the strength of individual synapses might not differ between genotypes.

Ocular Dominance Plasticity Is Increased in Both Juvenile and Adult Visual Cortex of KbDb KO Mice

Because there is a significant increase in cortical connectivity in KbDb KO mice present well past the critical period (P19–P32;

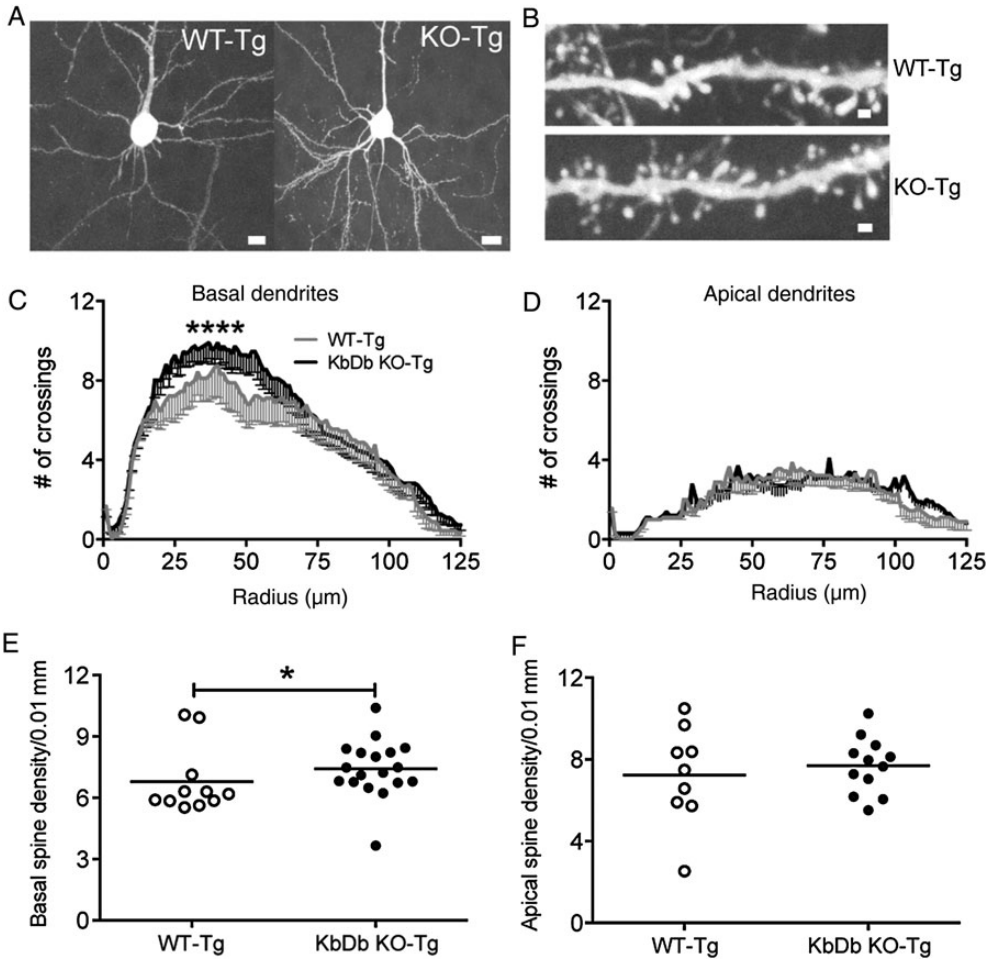

Figure 2. L2/3 pyramidal cell basal dendritic complexity and spine density are increased in KbDb KO-Tg. (*A*) Examples of GFP-labeled rabies-infected WT-Tg and KO-Tg L2/3 pyramids used for analysis. (*B*) Examples of WT-Tg and KO-Tg L2/3 basal dendrites and spines. (*C* and *D*) Sholl analysis of (*C*) basal and (*D*) apical dendritic branching in KbDb KO-Tg versus WT-Tg. Basal dendritic complexity is greater in KOs. $P < 0.0001$; two-way ANOVA; $n = 9$ WT-Tg and 11 KO-Tg cells. Apical dendritic complexity is similar between genotypes; $P = 0.21$; two-way ANOVA; $n = 9$ WT-Tg and 10 KO-Tg cells. Scale bar = 10 μm. (*E* and *F*) Spine density on L2/3 pyramids (*E*) basal and (*F*) apical dendrites. Basal, but not apical, dendritic spine density is elevated in KO-Tg. Basal dendrites: WT-Tg: 6.8 ± 0.5 spines/10 μm, $n = 11$ cells, 1990 total spines; KO-Tg: density = 7.4 ± 0.3 spines/10 μm; $n = 18$ cells, 3784 total spines; $P = 0.03$. $N = 7$ WT-Tg and 10 KO-Tg animals. Apical dendrites: WT-Tg: 7.2 ± 0.8 spines/10 μm, $n = 9$ cells, 1365 total spines; KO-Tg: density = 7.7 ± 0.4 spines/10 μm; $n = 12$ cells, 2399 total spines; $P = 0.84$. $N = 4$ WT-Tg and 7 KO-Tg animals. Scale bar = 1 μm. Each circle = one cell. *$P < 0.05$, ****$P < 0.0001$. Error bars = SEM. Analysis carried out at P40.

Gordon and Stryker 1996; Tagawa et al. 2005; Levelt and Hübener 2012), we wondered if there is also a change in OD plasticity that might even persist into adulthood. OD plasticity involves selective strengthening of synaptic inputs driven by the open eye and weakening of those driven by the closed eye in response to visual deprivation (Gordon and Stryker 1996), so an association between H2-Kb and H2-Db protein with synapses would be consistent with a role for these molecules in regulating plasticity. Therefore, we examined if H2-Kb and H2-Db protein is expressed in adult cortex. Previous work using antibodies of rather broad specificity showed that MHCI protein is localized to neurons and at synapses (Corriveau et al. 1998; Huh et al. 2000; Datwani et al. 2009; Needleman et al. 2010). Here, newly generated and specific antibodies to H2-Kb and H2-Db were used to probe protein expression levels in western blots of synaptosome preparations in juvenile and adult cortex. Results using an H2-Kb antibody and an H2-Kb/Db antibody show that protein for these particular MHCIs can be detected in synaptosomes, implying that they are expressed at or near synapses both during the critical period (P28) and in adult (P100; Fig. 4A).

OD plasticity in KbDb KO mice was assessed at P100, months after the end of the visual cortical critical period in mice (Gordon and Stryker 1996; Tagawa et al. 2005). Multiple methods are available to assess OD plasticity, including induction of the immediate early gene *Arc* (Hofer et al. 2006a, 2006b). *Arc* is rapidly transcribed in neurons firing action potentials (Lyford et al. 1995), and Arc mRNA visualization can be used as a spatial readout of neurons functionally responding to open eye stimulation (Tagawa et al. 2005). To assess OD plasticity, at P100, mice received 10 days of monocular enucleation (ME) and subsequently at P110 Arc mRNA induction was used to assess OD plasticity at the L3/4 border in visual cortex. The width of the Arc mRNA in situ hybridization signal along the L3/4 border in visual cortex ipsilateral to the open (non-deprived) eye was measured in WT versus KbDb KO mice; this width is a reliable measure of open eye strengthening, a key component of OD plasticity (Frenkel and Bear 2004; Tagawa et al. 2005). Following 10 days of ME, the width of Arc mRNA in situ hybridization signal in KbDb KO mice is significantly greater than in WT (WT ME: 4 mice, 1147 ± 45 μm; KbDb KO ME: 6 mice, 1334 ± 32 μm; $P = 0.02$; Fig. 4B,C). Note that, in WT mice, there is

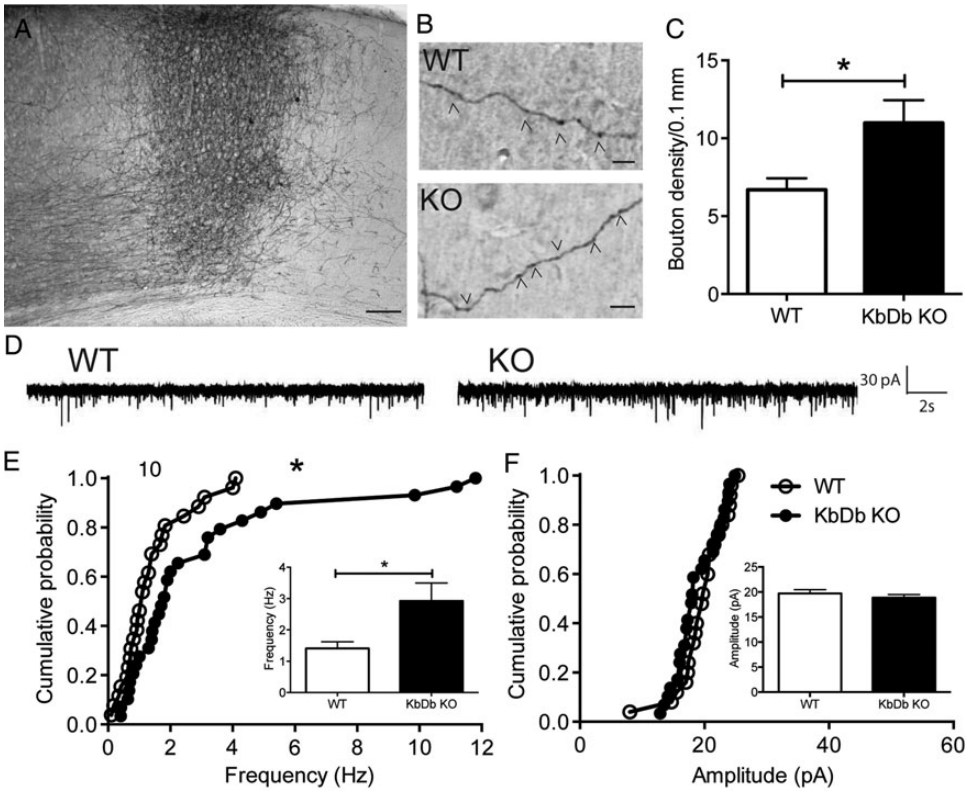

Figure 3. Bouton density and mEPSC frequency are elevated in KbDb KO L2/3 pyramidal cells. (*A–C*) Anterograde tracing of cortical axons following a BDA injection into visual cortex. (*A*) Representative image of labeled axons in a projection site ipsilateral to the injection. Scale bar = 100 μm. (*B*) Higher magnification view of WT and KO axons in L2/3 used for analysis. Arrowheads indicate boutons. Scale bars = 10 μm. (*C*) Histograms showing bouton density in KbDb KO versus WT. WT: 6.7 ± 0.7 boutons/100 μm; KO: 11.0 ± 1.5 boutons/100 μm, $P = 0.01$. $N = 9$ WT and 9 KO animals; 1028 WT and 1078 KO boutons. (*D–F*) Whole-cell recordings from L2/3 pyramidal neurons in WT versus KO visual cortex slices. (*D*) Representative traces of WT and KO mEPSC recordings. (*E* and *F*) Cumulative histograms of mEPSC (*E*) frequency and (*F*) amplitude. Frequency: WT: 1.4 ± 0.2 Hz; KO: 2.9 ± 0.6 Hz, $P = 0.02$. Amplitude: WT: 19.7 ± 0.7 pA; KO: 18.9 ± 0.7 pA, $P = 0.19$. $N = 26$ WT cells from 6 animals and 29 KO cells from 7 animals. Each circle = one cell. *$P < 0.05$. Error bars = SEM. Mann–Whitney *U*-test. Analysis carried out at P40.

almost no detectable change in the width of Arc mRNA signal following 10 days of ME [WT normally reared (NR) vs. WT ME; $P = 0.99$], consistent with the fact that the critical period ended months ago. Nor is there a difference between genotypes in NR mice not receiving visual deprivation (WT vs. KO NR; $P = 0.9996$; Fig. 4C). We also calculated a plasticity index, equal to the fold expansion of Arc signal following 10 days ME when compared with NR controls. The index is significantly greater for adult KbDb KO than for WT (WT: 1.01 ± 0.04, KbDb KO: 1.18 ± 0.03; $P = 0.002$; Fig. 4D), though it is lower than that seen during the critical period (from Datwani et al. 2009; WT: 1.51 ± 0.08, KbDb KO: 2.16 ± 0.11; $P < 0.001$). Thus, in KbDb KO visual cortex, OD plasticity as assessed by measuring open eye strengthening appears to persist into adulthood.

Discussion

A major finding of this study is that pyramidal neuron local and horizontal connectivity in visual cortex of KbDb KO mice, as assessed both anatomically and functionally, is significantly greater than in WT. We examined connectivity after the end of the critical period and observed that excitatory connections in visual cortex of KO are increased over WT, particularly long distance horizontal connections hundreds of microns away. In addition, KbDb KO L2/3 pyramids have more complex basal dendrites as well as slightly elevated basal dendritic spine density and axon bouton density. mEPSC frequency of L2/3 pyramids is also elevated, suggesting that overall functional excitatory connectivity is greater in KO visual cortex. These observations demonstrate that one or both of these MHC class I proteins regulate the spatial pattern and the number of pyramidal cell connections in visual cortex. Furthermore, these data combined with previous findings (Datwani et al. 2009; Lee et al. 2014) suggest that H2-Db and/or Kb contribute specifically to the process of activity-dependent dendritic sculpting and synapse pruning that normally occurs during the visual cortical critical period.

H2-Db and H2-Kb Regulate Intracortical Connectivity

Neuronal MHCI molecules were discovered in an unbiased screen for genes regulated by neural activity and visual experience (Corriveau et al. 1998), and H2-Kb and H2-Db are known to be needed for developmental synapse remodeling (Datwani et al. 2009; Glynn et al. 2011; Elmer et al. 2013) and pruning of retinogeniculate projections (Lee et al. 2014). H2-Db and H2-Kb are expressed in cortical pyramidal neurons (Huh et al. 2000; Datwani et al. 2009; Needleman et al. 2010; Adelson et al. 2012), detected in cortical synaptosomes as shown here, and thought to be at the cortical synapse as viewed in electron micrographs (Needleman et al. 2010). Because H2-Kb and H2-Db are present in cortex, we suggest that the failure to remodel intracortical connections is due to loss of function in the cortex, rather than in the LGN or retina. This suggestion is underscored by the important observation that retinal activity, as well as visual acuity, in KbDb KO mice is indistinguishable from

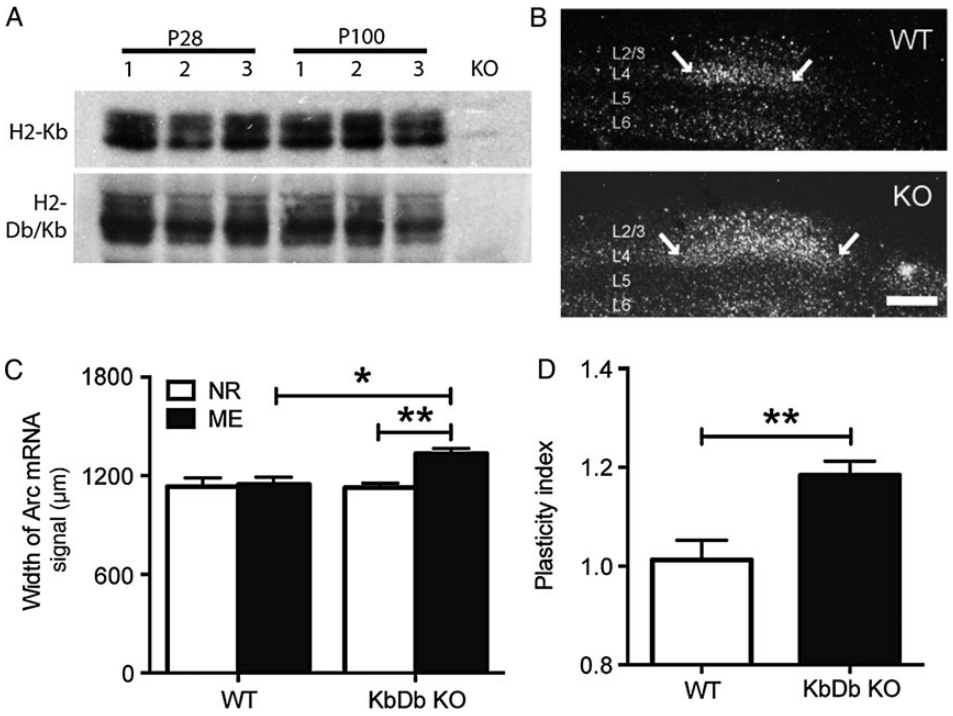

Figure 4. OD plasticity is enhanced in adult P100 KbDb KOs. (*A*) Western blot of synaptosome preparations from cortex using 2 different monoclonal antibodies, one recognizing exclusively H2-Kb (top panel) and the other recognizing both H2-Kb and H2-Db (bottom panel). H2-Kb and H2-Db protein can be detected in cortical synaptosomes in the adult (P100), as well as during the visual cortical critical period (P28). Each lane is loaded with a sample from one animal, with 3 animals per age examined. Note that no expression in KbDb KO control demonstrating antibody specificity. (*B*) Representative isotopic in situ hybridization images of Arc mRNA in the binocular zone of visual cortex ipsilateral to the open eye following 10 days of ME from P100 to P110. Arc mRNA signal (white dots = cells that have transcribed Arc mRNA) is upregulated in response to open eye stimulation in both WT and KO visual cortex, but occupies a wider region in KO (arrows). Layers are indicated. Scale bar = 100 μm. (*C*) Histograms showing changes in width of Arc mRNA signal measured at the L3/4 border in NR versus animals receiving 10 days of ME. WT NR: 4 animals, width of signal = 1133 ± 48 μm; WT ME: 4 animals, 1147 ± 45 μm; KO NR: 4 mice, 1127 ± 28 μm; KO ME: 6 mice, width = 1334 ± 32 μm. One-way ANOVA and Tukey's multiple comparison test. (*D*) Histograms comparing the plasticity index in adult KbDb KO mice versus WT. Plasticity index = width of Arc mRNA signal at L3/4 border in monocularly enucleated/NR animals. WT: 1.01 ± 0.04; KO: 1.18 ± 0.03; $P = 0.002$. Mann–Whitney *U*-test. $^{*}P < 0.05$, $^{**}P < 0.01$. Error bars = SEM. Analysis carried out at P110.

normal (Datwani et al. 2009; Lee et al. 2014). Thus, loss of neural activity, which might be expected to result in abnormal pruning, cannot explain the connectivity increases we observe here. Our observations are more consistent with the idea that Kb, Db, or both act downstream of activity as part of a pruning mechanism.

Results of our study correspond to and extend previous observations on a critical role for MHCI proteins in synapse elimination: In vitro, the frequency of mEPSCs and the density of synapses on rat cortical neurons can be modulated by expression of H2-Kb (a mouse MHCI gene) or by using beta 2 microglobulin (β2m) siRNA (Glynn et al. 2011). In vivo in single β2m knockout or double β2m/TAP1 knockout mice, the frequency of mEPSCs is elevated in juvenile cortex, and the density of synapses is increased in both juvenile and adult cortex and hippocampus, as assessed using transmission EM (Goddard et al. 2007; Glynn et al. 2011). These provide useful albeit indirect evidence for a role for H2-Kb or H2-Db in vivo specifically, because rat neurons express related but not identical MHC class I proteins to mice, and because β2m is an accessory molecule needed for stable surface expression of the majority (50+) of MHCI proteins (Zijlstra et al. 1990). In this study, we have examined mice lacking just 2 specific mouse MHCI molecules in vivo and observed not only an increase in functional synapses as assessed by mEPSC recordings, but also by directly examining spatial patterns of connectivity we have revealed an increase in excitatory pyramidal cell connectivity using the modified rabies virus transneuronal tracing method.

We further observed that dendritic complexity and spine density are elevated along proximal basal dendrites of L2/3 pyramids of KbDb KO visual cortex, but not along proximal apical dendrites. This selective effect on the basal dendrites of L2/3 cortical neurons in KbDb KO visual cortex is consistent with the fact that it is the basal rather than apical dendrites that receive the bulk of the intralaminar input from other L2/3 excitatory pyramids (Gilbert and Wiesel 1989; Thomson and Bannister 2003; Feldmeyer et al. 2006), as would be expected if each pyramidal neuron is receiving more input from other pyramidal neurons in KO versus WT. Other studies have shown that dendritic complexity and spine density can be regulated independently in apical versus basal dendrites. For example, neurotrophins have layer-specific and apical versus basal-specific effects (McAllister et al. 1995) and the secreted semaphorin 3A regulates L5 pyramid spine distribution and dendritic arborization via distinct holoreceptor complexes (neuropilin-2/plexin A3 affects spine number vs. neuropilin-1/plexin A4 affects basal dendritic arborization; Tran et al. 2009). We suggest that H2-Db and H2-Kb function to regulate basal dendritic complexity and spine density in L2/3 pyramidal neurons. However, we note that apical dendritic tufts in Layer 1 were not examined, and it is possible that H2-Db and H2-Kb could also contribute to the complexity and spine density there, without affecting the proximal apical dendrite.

Greater Connectivity in KbDb KO Mice Could Serve as a Substrate for Ocular Dominance Plasticity and Recovery From Injury

Increased excitatory connectivity could underlie the observed enhancement of open eye strengthening in KbDb KO mice,

following eye closure both in the critical period and in adult. Previous work has shown that, in WT mice, eye closure generates new dendritic spines on neurons in primary visual cortex (Keck et al. 2008; Hofer et al. 2009), and retinal lesions that silence part of visual cortex result in the formation of new intralaminar axonal arbors (Yamahachi et al. 2009; Marik et al. 2013). In particular, new spines formed on L5 apical dendrites during MD persist even if binocular vision is restored; then a second MD later in life leads to more rapid and pronounced OD plasticity than normally observed in adult (Hofer et al. 2006a, 2006b), without recruiting any additional spines (Hofer et al. 2009). These results suggest that experience creates an anatomical substrate for functional plasticity that can be accessed later on.

In support of this hypothesis, mice lacking the MHCI receptor PirB (paired immunoglobulin-like receptor B) also have elevated spine density on the apical dendrites of L5 pyramidal neurons in visual cortex (Djurisic et al. 2013), and this increase is accompanied by enhanced OD plasticity not only during the critical period, but also in adulthood (Syken et al. 2006; Djurisic et al. 2013). Here, we demonstrate exuberant connectivity that persists in KbDb KO visual cortex past the close of the critical period, as well as enhanced OD plasticity in adulthood. Other molecules that restrict adult OD plasticity include Lynx1, chondroitin sulfate proteoglycans (CSPGs), and Nogo/NgR (Pizzorusso et al. 2002; McGee et al. 2005; Morishita et al. 2010; Miyata et al. 2012). If structural changes underlie functional plasticity, it would be interesting to determine if the absence of these molecules also is associated with anatomical correlates such as increased spine density or altered spatial patterns of connectivity.

Structural and functional plasticity are needed for recovery from brain injury. H2-Kb and H2-Db therefore could be useful therapeutic targets. For example, we have reported that KO of both H2-Kb and H2-Db is neuroprotective in an adult stroke model, where KO mice have less cell death and better behavioral recovery (Adelson et al. 2012) and knock out of PirB receptor protects Alzheimer's model mice from memory loss (Kim et al. 2013). Defects in synapse pruning and plasticity during developmental critical periods have been hypothesized in disorders such as autism and Schizophrenia (Qiu et al. 2011; Glausier and Lewis 2013), and it is noteworthy that the human MHC class I locus has been strongly correlated with schizophrenia in genome-wide association studies (Ripke et al. 2013, 2014; Stefansson et al. 2014). Our observations here in mouse visual cortex make a firmer link between developmental circuit refinement, plasticity, and neuronal MHC class I function.

Authors' Contributions

J.D.A. and C.J.S. designed experiments. J.D.A. conducted circuit tracing, spine analysis, and dendritic branching experiments with input and reagents from K.M. and L.L. J.D.A. and R.W.S. conducted axon tracing experiments. J.D.A., S.C., and M.D. performed OD plasticity experiments. H.L. recorded mEPSCs. B.K.B. performed biochemistry. J.D.A. and C.J.S. discussed and analyzed data and wrote paper.

Supplementary Material

Supplementary material can be found at: http://www.cercor.oxfordjournals.org/.

Funding

This work was supported by the National Institutes of Health grants (MH07166 and EY02858), the Mathers Charitable Foundation, and the Ellison Foundation to C.J.S.; and a National Defense Science and Engineering Graduate Fellowship and National Science Foundation Graduate Research Fellowship to J.D.A.

Notes

We thank Shatz Lab members N. Sotelo, P. Kemper, and C. Chechelski for help with laboratory logistics and mice breeding, and G. Vidal for imaging training. We thank L. Schwarz from the Luo lab for the AAV TRE-mCherry-2a-TVA-2a-RG viral vector, and E. Callaway at the Salk Institute Viral Core for viruses. We also thank to H. Ploegh, MIT, for KbDb KO mice. *Conflict of Interest*: None declared.

References

Adelson JD, Barreto GE, Xu L, Kim T, Brott BK, Ouyang Y, Naserke T, Djurisic M, Xiong X, Shatz CJ, et al. 2012. Neuroprotection from stroke in the absence of MHCI or PirB. Neuron. 73 (6):1100–1107.

Barnard RJO, Elleder D, Young JAT. 2006. Avian sarcoma and leukosis virus-receptor interactions: from classical genetics to novel insights into virus-cell membrane fusion. Virology. 344(1):25–29.

Callaway EM, Katz LC. 1991. Effects of binocular deprivation on the development of clustered horizontal connections in cat striate cortex. Proc Natl Acad Sci USA. 88(3):745–749.

Callaway EM, Katz LC. 1990. Emergence and refinement of clustered horizontal connections in cat striate cortex. J Neurosci. 10(4):1134–1153.

Chen SX, Cherry A, Tari PK, Podgorski K, Kwong YKK, Haas K. 2012. The transcription factor MEF2 directs developmental visually drivin functional and structural metaplasticity. Cell. 151(1):41–55.

Cline HT. 2001. Dendritic arbor development and synaptogenesis. Curr Opin Neurobiol. 11(1):118–126.

Corriveau RA, Huh GS, Shatz CJ. 1998. Regulation of class I MHC gene expression in the developing and mature CNS by neural activity. Neuron. 21:505–520.

Datwani A, McConnell MJ, Kanold PO, Micheva KD, Busse B, Shamloo M, Smith SJ, Shatz CJ. 2009. Classical MHCI molecules regulate retinogeniculate refinement and limit ocular dominance plasticity. Neuron. 64:463–470.

De Marco García NV, Karayannis T, Fishell G. 2011. Neuronal activity is required for the development of specific cortical interneuron subtypes. Nature. 472(7343):351–355.

Djurisic M, Vidal GS, Mann M, Aharon A, Kim T, Santos AF, Zuo Y, Hübener M, Shatz CJ. 2013. PirB regulates structural substrate for cortical plasticity. Proc Natl Acad Sci USA. 110(51):20771–20776.

Durack JC, Katz LC. 1996. Development of horizontal projections in layer 2/3 of ferret visual cortex. Cereb Cortex. 6(2):178–183.

Elmer BM, Estes ML, Barrow SL, McAllister AK. 2013. MHCI requires MEF2 transcription factors to negatively regulate synapse density during development and in disease. J Neurosci. 33(34):13791–13804.

Elmer BM, McAllister AK. 2012. Major histocompatibility complex class I proteins in brain development and plasticity. Trends Neurosci. 35(11):660–670.

Feldmeyer D, Lübke J, Sakmann B. 2006. Efficacy and connectivity of intracolumnar pairs of layer 2/3 pyramidal cells in the barrel cortex of juvenile rats. J Physiol. 575:583–602.

Flavell SW, Greenberg ME. 2008. Signaling mechanisms linking neuronal activity to gene expression and plasticity of the nervous system. Annu Rev Neurosci. 31:563–590.

Frenkel MY, Bear MF. 2004. How monocular deprivation shifts ocular dominance in visual cortex of young mice. Neuron. 44(6):917–923.
Gilbert CD. 1992. Horizontal integration and cortical dynamics. Neuron. 9(1):1–13.
Gilbert CD, Wiesel TN. 1989. Columnar specificity of intrinsic horizontal and corticocortical connections in cat visual cortex. J Neurosci. 9(7):2432–2442.
Glausier JR, Lewis DA. 2013. Dendritic spine pathology in schizophrenia. Neuroscience. 251:90–107.
Glynn MW, Elmer BM, Garay PA, Liu X, Needleman LA, El-Sabeawy F, McAllister AK. 2011. MHCI negatively regulates synapse density during the establishment of cortical connections. Nat Neurosci. 14(4):442–453.
Goddard CA, Butts DA, Shatz CJ. 2007. Regulation of CNS synapses by neuronal MHC class I. Proc Natl Acad Sci USA. 104(16): 6828–6833.
Gordon JA, Stryker MP. 1996. Experience-dependent plasticity of binocular responses in the primary visual cortex of the mouse. J Neurosci. 16(10):3274–3286.
Hensch TK. 2005. Critical period plasticity in local cortical circuits. Nat Rev Neurosci. 6(11):877–888.
Hofer SB, Mrsic-Flogel TD, Bonhoeffer T, Hübener M. 2009. Experience leaves a lasting structural trace in cortical circuits. Nature. 457(7227):313–317.
Hofer SB, Mrsic-Flogel TD, Bonhoeffer T, Hübener M. 2006a. Lifelong learning: ocular dominance plasticity in mouse visual cortex. Curr Opin Neurobiol. 16(4):451–459.
Hofer SB, Mrsic-Flogel TD, Bonhoeffer T, Hübener M. 2006b. Prior experience enhances plasticity in adult visual cortex. Nat Neurosci. 9(1):127–132.
Hubel DH, Wiesel TN, LeVay S. 1977. Plasticity of ocular dominance columns in monkey striate cortex. Philos Trans Roy Soc B. 278(961):377–409.
Huberman AD, Feller MB, Chapman B. 2008. Mechanisms underlying development of visual maps and receptive fields. Annu Rev Neurosci. 31:479–509.
Huh GS, Boulanger LM, Du H, Riquelme PA, Brotz TM, Shatz CJ. 2000. Functional requirement for class I MHC in CNS development and plasticity. Science. 290:2155–2159.
Johnson MW, Chotiner JK, Watson JB. 1997. Isolation and characterization of synaptoneurosomes from single rat hippocampal slices. J Neurosci Meth. 77:151–156.
Katz LC, Shatz CJ. 1996. Synaptic activity and the construction of cortical circuits. Science. 274(5290):1133–1138.
Keck T, Mrsic-Flogel TD, Vaz Afonso M, Eysel UT, Bonhoeffer T, Hübener M. 2008. Massive restructuring of neuronal circuits during functional reorganization of adult visual cortex. Nat Neurosci. 11(10):1162–1167.
Kenan-Vaknin G, Ouaknine GE, Razon N, Malach R. 1992. Organization of layers II-III connections in human visual cortex revealed by in vitro injections of biocytin. Brain Res. 594(2): 339–342.
Kim T, Vidal GS, Djurisic M, William CM, Birnbaum ME, Garcia KC, Hyman BT, Shatz CJ. 2013. Human LilrB2 is a β-amyloid receptor and its murine homolog PirB regulates synaptic plasticity in an Alzheimer's model. Science. 341 (6152):1399–1404.
Knudsen EI. 2004. Sensitive periods in the development of the brain and behavior. J Cogn Neurosci. 16(8):1412–1425.
Lee H, Brott BK, Kirkby LA, Adelson JD, Cheng S, Feller MB, Datwani A, Shatz CJ. 2014. Synapse elimination and learning rules co-regulated by MHCI class I H2-D^{b}. Nature. 509 (7499):195–200.
Lein E, Shatz CJ. 2000. Rapid regulation of brain-derived neurotrophic factor mRNA within eye-specific circuits during ocular dominance formation. J Neurosci. 20(4):1470–1483.
Levelt CN, Hübener. 2012. Critical-period plasticity in the visual cortex. Annu Rev Neurosci. 35:310–330.
Livingstone MS, Hubel DH. 1984. Specificity of intrinsic connections in primate primary visual cortex. J Neurosci. 4(11): 2830–2835.
Lund JS, Yoshioka T, Levitt JB. 1993. Comparison of intrinsic connectivity in different areas of macaque monkey cerebral cortex. Cereb Cortex. 3(2):148–162.
Lyford GL, Yamagata K, Kaufmann WE, Barnes CA, Sanders LK, Copeland NG, Gilbert DJ, Jenkins NA, Lanahan AA, Worley PF. 1995. *Arc*, a growth factor and activity-regulated gene, encodes a novel cytoskeleton-associated protein that is enriched in neuronal dendrites. Neruon. 14(2):433–445.
Malach R, Amir Y, Harel M, Grinvald A. 1993. Relationship between intrinsic connections and functional architecture revealed by optical imaging and in vivo targeted biocytin injections in primate striate cortex. Proc Natl Acad Sci USA. 90(22):10469–10473.
Marik SA, Olsen O, Tessier-Lavigne M, Gilbert CD. 2013. Death receptor 6 regulates adult experience-dependent cortical plasticity. J Neurosci. 33(38):14998–15003.
McAllister AK, Lo DC, Katz LC. 1995. Neurotrophins regulate dendritic growth in developing visual cortex. Neuron. 15 (4):791–803.
McGee AW, Yang Y, Fischer QS, Daw NW, Strittmatter SM. 2005. Experience-driven plasticity of visual cortex limited by myelin and Nogo receptor. Science. 309:2222–2226.
Miyamichi K, Amat F, Moussavi F, Wang C, Wickersham I, Wall NR, Taniguchi H, Tasic B, Huang ZJ, He Z, et al. 2011. Cortical representations of olfactory input by trans-synaptic tracing. Nature. 472(7342):191–196.
Miyata S, Komatsu Y, Yoshimura Y, Taya C, Kitagawa H. 2012. Persistent cortical plasticity by upregulation of chondroitin 6-sulfation. Nat Neurosci. 15(3):414–422.
Morishita H, Miwa JM, Heintz N, Hensch TK. 2010. Lynx1, a cholinergic brake, limits plasticity in adult visual cortex. Science. 330 (6008):1238–1240.
Needleman LA, Liu XB, El-Sabeawy F, Jones EG, McAllister AK. 2010. MHC class I molecules are present both pre- and postsynaptically in the visual cortex during postnatal development and in adulthood. Proc Natl Acad Sci USA. 107: 16999–17004.
Nimchinsky EA, Sabatini BL, Svoboda K. 2002. Structure and function of dendritic spines. Annu Rev Physiol. 64:313–353.
Olavarria J, Van Sluyters RC. 1985. Organization and postnatal development of callosal connections in the visual cortex of the rat. J Comp Neurol. 239(1):1–26.
Osakada F, Callaway EM. 2013. Design and generation of recombinant rabies virus vectors. Nat Protoc. 8:1583–1601.
Palagina G, Eysel UT, Jancke D. 2009. Strengthening of lateral activation in adult rat visual cortex after retinal lesions captured with voltage-sensitive dye imaging in vivo. Proc Natl Acad Sci USA. 106:8743–8747.
Pizzorusso T, Medini P, Berardi N, Chierzi S, Fawcett JW, Maffei L. 2002. Reactivation of ocular dominance plasticity in the adult visual cortex. Science. 298:1248–1251.
Qiu S, Anderson CT, Levitt P, Shepherd GM. 2011. Circuit-specific intracortical hyperconnectivity in mice with deletion of the autism-associated Met receptor tyrosine kinase. J Neurosci. 31(15):5855–5864.

Ripke S, Neale BM, Corvin A, Walters JTR, Farh K, Holmans PA, Lee P, Bulik-Sullivan B, Collier DA, Huang H, et al. 2014. Biological insights from 108 schizophrenia-associated genetic loci. Nature. 511:421–427.

Ripke S, O'dushlaine C, Chambert K, Moran JL, Kahler AK, Akterin S, Bergen SE, Collins AL, Crowley JJ, Fromer M, et al. 2013. Genome-wide association analysis identifies 13 new risk loci for schizophrenia. Nat Genet. 45(10):1150–1159.

Ruthazer ES, Stryker MP. 1996. The role of activity in the development of long-range horizontal connections in area 17 of the ferret. J Neurosci. 16(22):7253–7269.

Salin PA, Bullier J. 1995. Corticocortical connections in the visual system: structure and function. Physiol Rev. 75(1):107–154.

Sato M, Stryker MP. 2008. Distinctive features of adult ocular dominance plasticity. J Neurosci. 28(41):10278–10286.

Shatz CJ. 1990. Impulse activity and the patterning of connections during CNS development. Neuron. 5:745–756.

Shatz CJ. 2009. MHC class I: an unexpected role in neuronal plasticity. Neuron. 64:40–45.

Sholl DA. 1953. Dendritic organization in the neurons of the visual and motor cortices of the cat. J Anat. 87(4):387–406.

Sin WC, Haas K, Ruthazer ES, Cline HT. 2002. Dendrite growth increased by visual activity requires NMDA receptor and Rho GTPases. Nature. 419:475–480.

Stefansson H, Meyer-Lindenberg A, Steinberg S, Magnusdottir B, Morgen K, Arnarsdottir S, Bjornsdottir G, Walters GB, Jonsdottir GA, Doyle OM, et al. 2014. CNVs conferring risk of autism or schizophrenia affect cognition in controls. Nature. 505(7483):361–366.

Syken J, Grandpre T, Kanold PO, Shatz CJ. 2006. PirB restricts ocular-dominance plasticity in visual cortex. Science. 313:1795–1800.

Tagawa Y, Kanold PO, Majdan M, Shatz CJ. 2005. Multiple periods of functional ocular dominance plasticity in mouse visual cortex. Nat Neurosci. 8(3):380–388.

Tanigawa H, Wang Q, Fujita I. 2005. Organization of horizontal axons in the inferior temporal cortex and primary visual cortex of the macaque monkey. Cereb Cortex. 15 (12):1887–1899.

Thomson AM, Bannister AP. 2003. Interlaminar connections in the neocortex. Cereb Cortex. 13(1):5–14.

Trachtenberg JT, Stryker MP. 2001. Rapid anatomical plasticity of horizontal connections in the developing visual cortex. J Neurosci. 21(10):3476–3482.

Tran TS, Rubio ME, Clem RL, Johnson D, Case L, Tessier-Lavigne M, Huganir RL, Ginty DD, Kolodkin AL. 2009. Secreted semaphorins control spine distribution and morphogenesis in the postnatal CNS. Nature. 462(7276):1065–1069.

Tropea D, Van Wart A, Sur M. 2009. Molecular mechanisms of experience-dependent plasticity in visual cortex. Proc Natl Acad Sci USA. 364:341–355.

Vaillant AR, Zanassi P, Walsh GS, Aumont A, Alonso A, Miller FD. 2002. Signaling mechanisms underlying reversible activity-dependent dendrite formation. Neuron. 34(6):985–998.

Van Hooser SD, Heimel JA, Chung S, Nelson SB. 2006. Lack of patchy horizontal connectivity in primary visual cortex of a mammal without orientation maps. J Neurosci. 26 (29):7680–7692.

Veenman CL, Reiner A, Honig MG. 1992. Biotinylated dextran amine as an anterograde tracer for single- and double-labeling studies. J Neurosci Meth. 41(3):239–254.

Vugmeyster Y, Glas R, Pérarnau B, Lemonnier FA, Eisen H, Ploegh H. 1998. Major histocompatibility complex (MHC) class I $KbDb^{-/-}$ deficient mice possess functional $CD8^{+}$ T cells and natural killer cells. Proc Natl Acad Sci USA. 95 (21):12492–12497.

Wall NR, Wickersham IR, Cetin A, De La Parra M, Callaway EM. 2010. Monosynaptic circuit tracing in vivo through Cre-dependent targeting and complementation of modified rabies virus. Proc Natl Acad Sci USA. 107(50):21848–21853.

Wickersham IR, Finke S, Conzelmann K, Callaway EM. 2007. Retrograde neuronal tracing with a deletion-mutant rabies virus. Nat Methods. 4(1):47–49.

Wiesel TN, Hubel DH. 1963. Single-cell responses in striate cortex of kittens deprived of vision in one eye. J Neurophysiol. 26:1003–1017.

Yamahachi H, Marik SA, McManus JN, Denk W, Gilbert CD. 2009. Rapid axonal sprouting and pruning accompany functional reorganization in primary visual cortex. Neuron. 64:719–729.

Yin Y, Edelman GM, Vanderklish PW. 2002. The brain-derived neurotrophic factor enhances synthesis of Arc in synaptoneurosomes. Proc Natl Acad Sci USA. 99:2368–2373.

Yuste R, Bonhoeffer T. 2001. Morphological changes in dendritic spines associated with long-term synaptic plasticity. Annu Rev Neurosci. 24:1071–1089.

Zijlstra M, Bix M, Simister NE, Loring JM, Raulet DH, Jaenisch R. 1990. β2-Microglobulin deficient mice lack $CD4\text{-}8^{+}$ cytolytic T cells. Nature. 344:742–746.